NEOPLASIA
www.neoplasia.com

Volume 12 Number 8 August 2010 pp. 608–617 608

Hypoxic Tumor Microenvironments Reduce Collagen I Fiber Density[1]

Samata M. Kakkad*, Meiyappan Solaiyappan*, Brian O'Rourke†, Ioannis Stasinopoulos*, Ellen Ackerstaff*,[2], Venu Raman*, Zaver M. Bhujwalla* and Kristine Glunde*

*JHU ICMIC Program, Russell H. Morgan Department of Radiology and Radiological Science, The Johns Hopkins University School of Medicine, Baltimore, MD, USA; †Institute of Molecular Cardiobiology, The Johns Hopkins University School of Medicine, Baltimore, MD, USA

Abstract

Although the mechanisms through which hypoxia influences several phenotypic characteristics such as angiogenesis, selection for resistance to apoptosis, resistance to radiation and chemotherapy, and increased invasion and metastasis are well characterized, the relationship between tumor hypoxia and components of the extracellular matrix (ECM) is relatively unexplored. The collagen I (Col1) fiber matrix of solid tumors is the major structural part of the ECM. Col1 fiber density can increase tumor initiation, progression, and metastasis, with cancer cell invasion occurring along radially aligned Col1 fibers. Here we have investigated the influence of hypoxia on Col1 fiber density in solid breast and prostate tumor models. Second harmonic generation (SHG) microscopy was used to detect differences in Col1 fiber density and volume between hypoxic and normoxic tumor regions. Hypoxic regions were detected by fluorescence microscopy, using tumors derived from human breast and prostate cancer cell lines stably expressing enhanced green fluorescent protein (EGFP) under transcriptional control of the hypoxia response element. In-house fiber analysis software was used to quantitatively analyze Col1 fiber density and volume from the SHG microscopy images. Normoxic tumor regions exhibited a dense mesh of Col1 fibers. In contrast, fewer and structurally altered Col1 fibers were detected in hypoxic EGFP-expressing tumor regions. Microarray gene expression analyses identified increased expression of lysyl oxidase and reduced expression of some matrix metalloproteases in hypoxic compared with normoxic cancer cells. These results suggest that hypoxia mediates Col1 fiber restructuring in tumors, which may impact delivery of macromolecular agents as well as dissemination of cells.

Neoplasia (2010) 12, 608–617

Introduction

Tumors display hypoxic environments that primarily arise from their abnormal and chaotic vasculature [1]. Hypoxia triggers multiple signaling cascades that significantly affect biologic outcomes including angiogenesis, selection for resistance to apoptosis, resistance to radiation and chemotherapy, and increased invasion and metastasis [2,3]. The extracellular matrix (ECM) plays an important role in drug delivery as well as invasion and metastasis, but

Abbreviations: Col1, collagen I; ECM, extracellular matrix; EGFP, enhanced green fluorescent protein; FOV, field of view; HIF, hypoxia-inducible factor; HRE, hypoxia response element; LOX, lysyl oxidase; MMP, matrix metalloproteinase; pro-Col1, procollagen type I; ROI, region of interest; SHG, second harmonic generation; uPA, urokinase plasminogen activator; uPAR, urokinase plasminogen activator receptor

Address all correspondence to: Kristine Glunde, PhD, Russell H. Morgan Department of Radiology and Radiological Science, Johns Hopkins University School of Medicine, 212 Traylor Bldg., 720 Rutland Ave, Baltimore, MD 21205. E-mail: kglunde@mri.jhu.edu or Zaver M. Bhujwalla, PhD, Russell H. Morgan Department of Radiology and Radiological Science, Johns Hopkins University School of Medicine, 208C Traylor Bldg, 720 Rutland Ave, Baltimore, MD 21205. E-mail: zaver@mri.jhu.edu

[1]This work was supported by the National Institutes of Health grants P50 CA103175, P30 CA006973, and R01 CA82337.

[2]Current address: Department of Medical Physics, Memorial Sloan-Kettering Cancer Center, New York, NY 10065.

Received 1 March 2010; Revised 26 May 2010; Accepted 27 May 2010

DOI 10.1593/neo.10344

the relationship between tumor hypoxia and ECM components is relatively unexplored.

The ECM in breast and prostate tumors is composed of a complex meshwork of fibrillar collagens, glycoproteins, and proteoglycans [4,5], which profoundly affect metastasis, as well as proliferation, angiogenesis, adhesion, migration, invasion, and drug delivery [4–9]. Collagen I (Col1) fibers are the major structural ECM component in breast [4,10–12] and prostate tumors [8,13,14]. A recent study demonstrated a causal relationship between Col1 fibers and metastasis in a bitransgenic mouse model with increased stromal Col1, in which high Col1 fiber density was able to significantly increase mammary tumor initiation, progression, and lung metastasis [11]. Cancer cell invasion in this mouse model started at the tumor-stromal interface in the primary tumor along radially aligned Col1 fibers [10]. The presence of a fibrotic focus in central tumor regions of breast cancer patients has been suggested as a prognostic factor and surrogate marker for hypoxia in breast tumors [15,16]. A recent study in a carcinogen-induced rat mammary carcinoma model indicated that, overall, more fibrotic tumors were also more hypoxic [17]. Cells of myofibroblast phenotype in the reactive stroma of Gleason 3–scored prostate cancers exhibited an elevated Col1 synthesis, which was first observed in activated peri-acinar fibroblasts adjacent to prostatic intraepithelial neoplasia [8].

Col1 fiber biosynthesis, maturation, and deposition is a multistep process, initiated by the *Col1A1* and *Col1A2* genes that produce the pro-α1(I) and pro-α2(I) chains, respectively, of procollagen type I (pro-Col1). Intracellular prolyl-3/4-hydroxylases, lysyl hydroxylases, and protein disulfide isomerases further modify these pro-α1(I) and pro-α2(I) chains to form pro-Col1 triple helices [18,19]. Fibroblasts are primarily responsible for synthesizing and secreting pro-Col1, whereas hepatic stellate cells [20], osteoblasts [21], odontoblasts [21], and hypoxic smooth muscle cells [22] also have the ability to produce pro-Col1. Extracellular procollagen N- and C-proteinases cleave the pro-Col1 propeptide ends of secreted pro-Col1, thereby initiating the self-assembly of collagen microfibrils [19]. Extracellular lysyl oxidase (LOX) covalently cross-links Col1 microfibrils with each other to form strong and stable mature Col1 fibers that surround cells within the ECM [19]. Fibrillar Col1 profoundly affects the mechanical properties of tissues, with high Col1 fiber content corresponding to more rigid and less compressible tissue properties [19]. Breast [23,24] and prostate cancer cells [8] can stimulate Col1 synthesis in tumor-associated fibroblasts and reorganize a previously random Col1 fiber matrix [10]. In addition, Col1 fibers in breast and prostate tumors can be degraded and remodeled by matrix metalloproteinase (MMP)-1 and MMP-14 (also referred to as MT1-MMP), which are secreted by or located on the cancer cells [25]. Whereas MMP-1 and MMP-14 initiate Col1 fiber degradation in the tumor microenvironment, further breakdown is mediated by MMP-2, MMP-9, MMP-12, and MMP-13 [26,27], as well as cathepsins and the urokinase plasminogen activator (uPA) and uPA receptor (uPAR) system [28].

In normal tissues, hypoxic environments promote the formation of collagen deposits [18,29,30]. The influence of hypoxia on Col1 remodeling in solid tumors *in vivo* is relatively unexplored. The purpose of our study was to determine the effect of hypoxia on Col1 fibers in solid breast and prostate tumor models.

We used second harmonic generation (SHG) microscopy to detect Col1 fibers in these tumor models. SHG microscopy detects the intrinsic signal of the noncentrosymmetric physical properties of Col1 fibers without an exogenous optical imaging agent [31,32]. SHG microscopy has been previously used in tumor xenografts to assess ECM integrity [31]. With SHG microscopy of human specimens, Col1 fibers in breast tumors were found to be straighter and denser than the fibers in benign lesions or normal breast tissue [32]. Here, for the first time, we have applied SHG microscopy to detect differences in Col1 fibers between hypoxic and normoxic tumor regions. The studies were performed using tumors derived from human breast and prostate cancer cell lines stably expressing enhanced green fluorescent protein (EGFP) under transcriptional control of five copies of a hypoxia response element (HRE), which have already been used in several studies in our laboratory [33,34]. To analyze Col1 fiber density and volume from the SHG microscopy images, we developed an in-house fiber analysis software. Normoxic tumor regions without fluorescence exhibited a dense mesh of Col1 fibers, whereas fewer and structurally altered Col1 fibers were detected in hypoxic EGFP-expressing tumor regions. Microarray gene expression analyses indicated increased LOX expression and reduced expression of MMPs in hypoxic cancer cells. These results suggest that tumor hypoxia can result in Col1 fiber restructuring, which may influence several ECM-related characteristics such as macromolecular transport and cancer cell dissemination.

Materials and Methods

Cell Lines and Tumor Models

The triple-negative metastatic human breast cancer cell line MDA-MB-231 [35] and the androgen-independent human prostate cancer cell line PC-3 [36] were obtained from the American Type Culture Collection (ATCC, Rockville, MD). Wild-type MDA-MB-231 [37] and PC-3 [38] cells were maintained as previously described. To generate MDA-MB-231 and PC-3 cells that express EGFP under hypoxic conditions as a hypoxia-inducible factor 1 (HIF-1)–driven hypoxia sensor, MDA-MB-231 and PC-3 cells were stably transfected with a construct containing five copies of the HRE of the human *VEGF-A* gene ligated to the complementary DNA of EGFP, which produced MDA-MB-231–5HRE-EGFP and PC-3–5HRE-EGFP as previously described [33,34]. EGFP expression was verified in hypoxic cell cultures by fluorescence microscopy and in corresponding protein lysates by sodium dodecyl sulfate–polyacrylamide gel electrophoresis and immunoblot analysis with anti-EGFP antibody (BD Biosciences, San Jose, CA) as previously described [33,34]. In our previous studies, we observed detectable EGFP expression within 6 hours of exposure to less than 1% O_2 and robust EGFP expression by 20 hours in HRE-EGFP–expressing cells in culture [33]. Cells were routinely characterized for hypoxia–driven EGFP expression before inoculation in mice.

Two million MDA-MB-231–5HRE-EGFP cells were orthotopically inoculated in the mammary fat pad of anesthetized female severe combined immunodeficient mice as previously described [39] to grow solid MDA-MB-231–5HRE-EGFP xenografts. Solid PC-3–5HRE-EGFP prostate tumor xenografts were obtained by inoculating 2×10^6 PC-3–5HRE-EGFP cells in 0.1 ml of Hank's balanced salt solution (Sigma-Aldrich, St Louis, MO) subcutaneously in the right flank of male severe combined immunodeficient mice [33,34]. Tumor xenografts reached their final experimental size within 8 weeks. In our previous studies, low oxygen tension was detected in several EGFP-fluorescing regions ($Po_2 < 0.6$ mm Hg), and higher oxygen tensions (5.0 mm Hg < Po_2 < 40.0 mm Hg) comparable to normal muscle tissue (23.0 mm Hg < Po_2 < 50.0 mm Hg) were detected in several nonfluorescing peripheral tumor regions measured with a fiber-optic oxygen probe inserted *in vivo* [33].

SHG and Confocal Microscopy

Animals were killed, tumor xenografts were excised for *ex vivo* fluorescence microscopy, and three to five serial 2-mm-thick fresh tissue slices were cut using an acrylic adjustable tissue slicer (12 mm depth up to 25 mm width; Braintree Scientific, Inc, Braintree, MA) and tissue slicer blades (Braintree Scientific, Inc). These serial fresh xenograft tissue slices were each placed on individual microscope slides (Fisherbrand catalog number 12-550-34; Fisher Scientific, Pittsburgh, PA), which were stored in a box containing ice on the bottom, in which the slides were located on a perforated plate at approximately 1 cm above the ice to ensure a tissue temperature of approximately 4°C to avoid tissue degradation. For microscopic measurements, a given slide holding a tumor slice was taken out of the icebox and placed under the microscope for the time of microscopic imaging. In between microscopic measurements, the fresh tumor slices were returned to the icebox to keep the tissue at 4°C, and they were periodically moistened with saline to avoid dehydration of the tissue. EGFP expression in these tumor slices was detected by fluorescence microscopy using a 1× objective attached to a Nikon inverted microscope, equipped with a filter set for 450 to 490 nm excitation and 500 to 550 nm emission, and a Nikon Coolpix digital camera (Nikon Instruments, Inc, Melville, NY). These 1× images were used to coarsely locate hypoxic and normoxic tumor regions in subsequent SHG microscopic acquisitions.

For SHG microscopy, a microscope slide holding a fresh 2-mm-thick tissue slice was removed from the icebox and placed under the objective of a multiphoton system. After SHG microscopy, the slide was moistened and returned to the icebox. The SHG microscopy of tumor slices was performed on a Nikon/Bio-Rad or a Zeiss LSM 710 NLO Meta multiphoton microscopy system (Carl Zeiss MicroImaging, Inc, Thornwood, NY). The Nikon E600FN upright research fluorescence microscope was equipped with a Bio-Rad MRC-1024/2-P multiphoton attachment (Bio-Rad, Hercules, CA) and a Tsunami 3941 M1S femtosecond mode-locked Ti:Sa pulsed laser (Spectra Physics, Mountain View, CA) pumped by a 10-W Millenia X solid-state laser (Spectra Physics). Laser light of 880 nm was used as an incident light for generation of the SHG Col1 signal and for two-photon excitation of EGFP fluorescence. The SHG signal from Col1 fibers was detected at 410 to 470 nm, and the EGFP fluorescence was detected at 500 to 560 nm. The Zeiss 710 NLO Meta confocal microscope (Carl Zeiss MicroImaging, Inc) was equipped with a 680- to 1080-nm tunable Coherent Chameleon Vision II laser (Coherent, Inc, Santa Clara, CA). For SHG Col1 microscopy, incident laser light at 880 nm was used, and the SHG signal was detected at 410 to 470 nm. Simultaneously, EGFP was excited with the 488-nm laser line and detected at 500 to 560 nm. On both microscope systems, a 25× lens was used to acquire confocal *z*-stacks of approximately 100 μm thickness with a *z*-interval of approximately 5 μm. Neither the SHG nor the EGFP signal of a given field of view (FOV) on a given tumor tissue slice changed over time when imaging the same FOV multiple times within one imaging session, for example, once in the beginning and once at the end of an imaging session.

After microscopy, fresh tumor slices were frozen in Tissue Tek OCT freezing compound (Sakura Finetek USA, Inc, Torrance, CA). Frozen slices were cryosectioned with a microcryotome (Microm International, Walldorf, Germany) at 100 μm thickness, fixed with 3% paraformaldehyde (Sigma-Aldrich) solution, stained for nuclei with Hoechst 33342 (Invitrogen Corp, Carlsbad, CA), and mounted with Faramount aqueous mounting medium (DakoCytomation, Carpinteria, CA). Two-photon excitation of Hoechst 33342 at 880 nm together with excitation of the SHG signal was performed on these whole-mount sections. Hoechst was detected at 450 to 500 nm, and the SHG Col1 signal was detected at 400 to 450 nm. EGFP was single-photon excited at 488 nm and detected at 500 to 560 nm.

Image and Statistical Analysis

Image analysis to quantify (1) the Col1 fiber distance distribution and (2) the Col1 fiber volume was performed using in-house software. This software was written in Matlab using MATLAB 7.4.0 (The MathWorks, Natick, MA) and described in detail in the Results section. Regions of interest (ROIs) containing defined percentages of hypoxic EGFP-fluorescing cells were drawn and analyzed with this software. A one-sided *t* test ($\alpha = 0.05$) was used to detect significant differences between hypoxic and normoxic ROIs using Microsoft Office Excel 2007 (Microsoft, Redmond, WA). *P* values < .05 were considered to be significant.

Gene Expression Analysis with Affymetrix Microarrays of Hypoxic versus Normoxic Cells

Wild-type MDA-MB-231 and PC-3 cells were exposed to hypoxic conditions in a commercially available culture chamber (BioSpherix Ltd, Redfield, NY) for 24 and 48 hours. This humidified culture chamber was maintained at 37°C and equilibrated with a mixture of 0.3% to 0.7% O_2 and 5% CO_2 for the required time intervals, using controlled N_2 and CO_2 gas infusions (BioSpherix). Controls were placed in a standard cell culture incubator at 37°C in a humidified atmosphere containing 21% O_2 and 5% CO_2. Total cellular RNA was isolated from approximately 10^7 cells, using the RNeasy Mini Kit (Qiagen, Inc, Valencia, CA) and QIAshredder homogenizer spin columns (Qiagen) as previously described [37]. The microarray hybridization was performed at the Johns Hopkins Medical Institution's Microarray Core Facility using the Human Genome U133 Plus 2.0 GeneChip array (Affymetrix, Inc, Santa Clara, CA) and the Affymetrix GeneChip platform, Agilent GeneArray Scanner, and Micro Array Suite 5.0 software by Affymetrix as previously described [37]. To estimate the gene expression signals, data analysis was conducted on the chips' cell intensity file probe signal values at the Affymetrix probe pair (perfect match probe and mismatch probe) level, using statistical techniques and the robust multiarray analysis package as previously described [37,40,41]. The posterior probabilities of the differential expression of genes were estimated for hypoxic *versus* normoxic MDA-MB-231 cells and hypoxic *versus* normoxic PC-3 cells. The criterion of the posterior probability > .5, which means the posterior probability is larger than by chance, was used to produce the differentially expressed gene lists. All computations were performed under the *R* environment as previously described [37].

Results

To achieve quantitative analysis of Col1 fibers from SHG images, we developed in-house image analysis software. A major challenge in the quantitative analysis of Col1 fiber distribution and volume occurs because of the complex intersecting patterns of the fibers in three spatial dimensions, which is apparent in the raw data set of *z*-sections in Figure 1. We therefore developed a practical and intuitive approach to characterize these distribution patterns by analyzing the interstices in the fibrillar mesh outlined in Figure 2. The analytical approach presented in Figure 2 was applied to quantify the Col1 fiber distances and volumes from tumor xenograft models. Figure 2*A* shows the representative raw image displayed as a *z*-projection of the three-dimensional data set, which was generated from the *z*-sections in Figure 1. Figure 2*B* shows that the software was able to detect hypoxic cells independent of

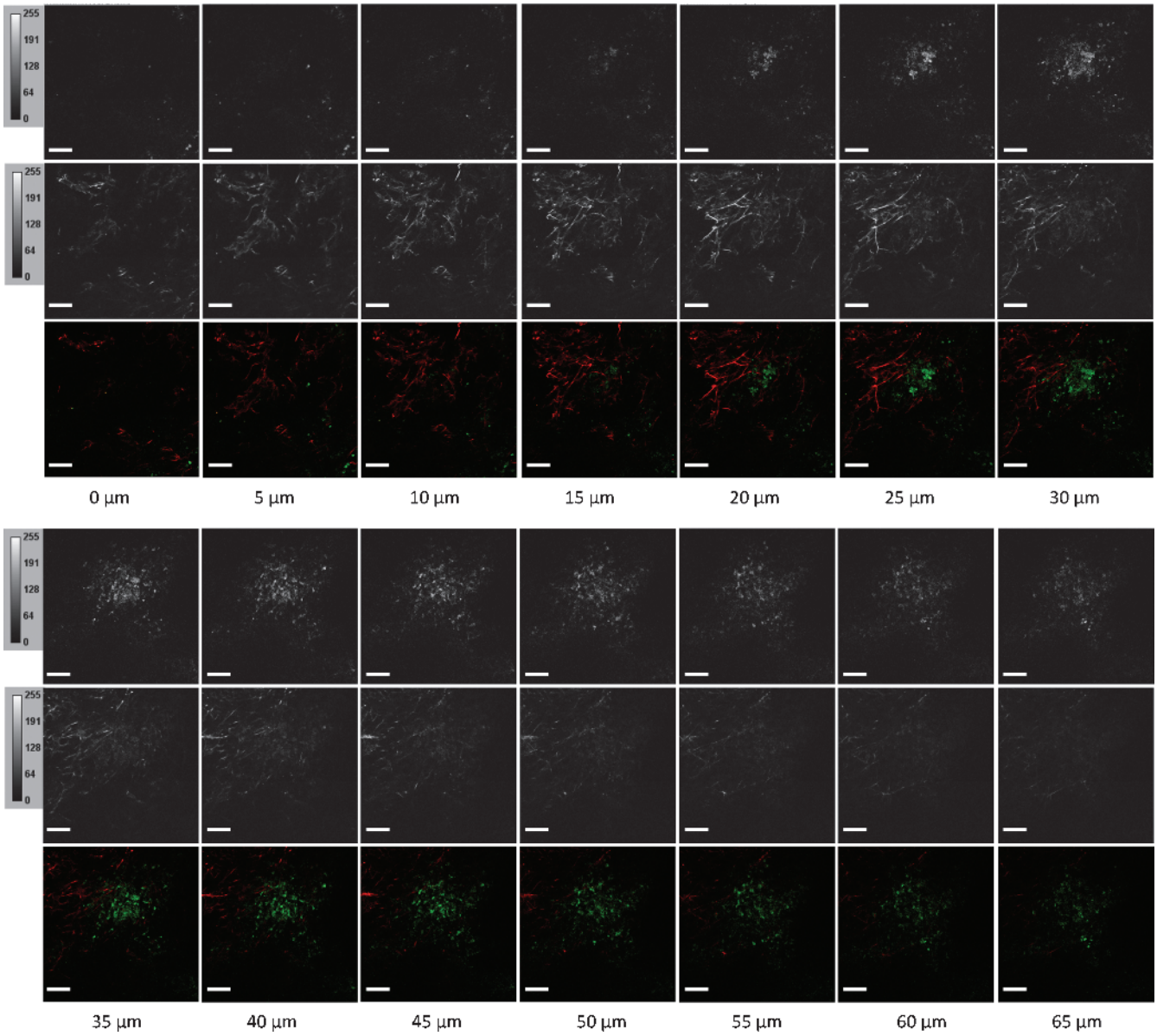

Figure 1. Complete representative raw data set showing the *z*-series of EGFP images (top panel) and SHG images (middle panel) in gray scale, as well as the merged images displaying the EGFP channel in green and the SHG channel in red. Scale bars, 100 μm.

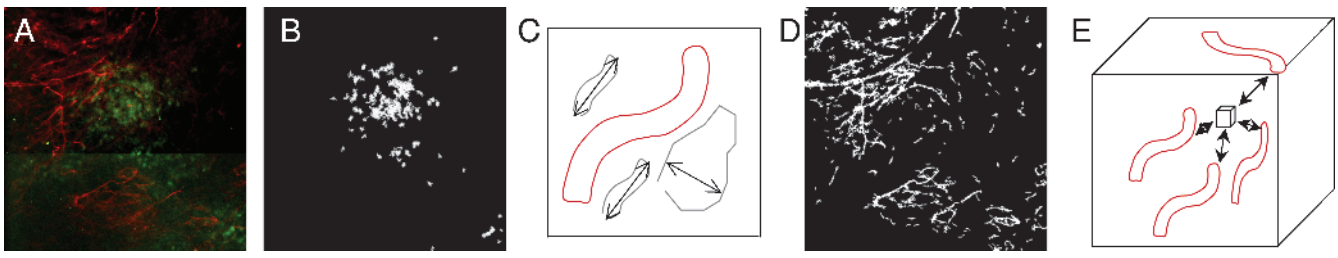

Figure 2. Quantification of fiber distance distribution with in-house software: (A) representative raw image data shown as *z*-projection of the Col1 fibers (red) in a hypoxic (green) region; (B) representative example of software detection of hypoxic cells (green in raw image (A)) independent of fluorescence intensity and threshold of raw images; preprocessing using the filter (C) to identify fiber-like objects (red) among various non–fiber-like objects in the image to produce (D) the corresponding Col1 fiber image; (E) computing the distances three-dimensionally to the surrounding fibers from each voxel to determine the nearest distance to a fiber. The fiber volume is computed as an additional parameter.

variability in the dynamic range of the green fluorescence signal in the images. The hypoxic ROIs in our analysis were defined as containing more than 80% green fluorescing hypoxic cells; normoxic regions contained less than 1% of green fluorescing hypoxic cells in the ROI. Images were preprocessed to exclude noise and nonfibrillar shapes as shown in Figure 2*C*. Figure 2*D* shows that the software detected Col1 fiber structures from the raw image. A three-dimensional volume of the Col1 fiber mesh within a given ROI was selected, and Euclidean distances from each empty voxel to the nearest Col1 fiber voxel were computed to quantify the fiber distances within the mesh (Figure 2*E*). This provided a cumulative histogram of the distance distribution as a measure of porosity of the mesh as shown in the subsequent figures. In addition, a second parameter, the Col1 fiber volume, was quantified using our in-house three-dimensional image quantification software. Figure 3 shows the performance of this software on an artificial training data set. We manually generated a sparser fiber image A as shown in Figure 3*A*, which was modified in Figure 3*B* with a few additional lines representing fibers to give image B. Our software was able to correctly detect a shift toward a denser fiber distribution (Figure 3*C*) and an increased fiber volume (Figure 3*D*) for image B compared with image A. Compared with analysis methods based on Fourier analysis [32], our method derived parameters that are visually evident in the images. Because of its robustness, the method requires minimal preprocessing steps that can be adopted to varying image quality.

A representative example from an MDA-MB-231 breast tumor is shown in Figure 4 and that from a PC-3 prostate tumor is shown in Figure 5. Low-power microscopic images covering 2-mm-thick tumor slices from representative MDA-MB-231–5HRE-EGFP (Figure 4*A*) and PC-3–5HRE-EGFP (Figure 5*A*) tumors demonstrated that the hypoxic green fluorescing regions were heterogeneously distributed throughout the tumors. Figures 4*A* and 5*A* show the corresponding bright-field, EGFP fluorescence, and overlay of bright-field and fluorescence images from left to right. Hypoxic regions of MDA-MB-231 breast as well as PC-3 prostate tumor xenografts displayed significantly sparser, more porous Col1 fibers than normoxic regions as evident from representative microscopic images of normoxic (Figures 4*B* and 5*B*) and hypoxic regions (Figures 4*C* and 5*C*). Figures 4, *B* and *C*, and 5, *B* and *C*, show *z*-projections of the *z*-stack on the left and the corresponding three-dimensional display of the image on the right. The median hypoxic Col1 interfiber distances were significantly (P = .050 for MDA-MB-231, n = 3-5; P = .002 for PC-3, n = 9) higher compared with the median normoxic Col1 interfiber distances for both breast (Figure 4*D*, n = 3-5 ROIs) and prostate tumor xenografts (Figure 5*D*, n = 9 ROIs). Cumulative histograms of the Col1 fiber distance distributions of breast (Figure 4*D*) and prostate (Figure 5*D*) tumor xenografts demonstrated that the mean Col1 fiber distance distribution shifted toward longer interfiber distances in hypoxic compared with normoxic regions. This increased Col1 fiber distance in hypoxic tumor areas implied a more porous distribution of Col1 fibers in hypoxic *versus* normoxic tumor regions. The Col1 fiber volume was significantly lower (breast tumor model: P = .0428, n = 3-5 ROIs in Figure 4*E*; prostate tumor model: P = .0004, n = 9 ROIs in Figure 5*E*) in hypoxic than in normoxic regions in both tumor models, consistent with the fewer, more porous distribution of Col1 fibers in hypoxic tumor regions. Using Hoechst 33342 staining and fluorescence microscopic detection of cell nuclei, we confirmed that an equal number of cells and comparable cell density were present in hypoxic and normoxic regions of MDA-MB-231 and PC-3 tumor xenografts, as shown in representative images from MDA-MB-231 tumors in Figure 6.

We investigated differences in gene expression of factors secreted by hypoxic *versus* normoxic cancer cells that can influence Col1 synthesis, cross-linking, and degradation. A comparison of gene expression analyzed using Affymetrix Human Genome U133 Plus 2.0 GeneChip arrays of hypoxic *versus* normoxic cells for MDA-MB-231 breast cancer cells is shown in Table 1 and that for PC-3 prostate cancer cells is shown in Table 2. Both cancer cell types showed increased expression of LOX under hypoxic conditions in cell culture. In addition, some MMPs were underexpressed under hypoxic conditions, such as MMP-3 in MDA-MB-231 breast cancer cells and MMP-1 and MMP-16 in prostate cancer cells. The uPAR was overexpressed in hypoxic PC-3 cells compared with normoxic controls. Other than the reported genes, no differences were detected in any other MMPs, cathepsins, tissue inhibitors of metalloproteases, or genes involved in Col1 synthesis and degradation. Additional studies are currently underway to elucidate the molecular differences leading to the changes on Col1 fiber patters in hypoxic compared with normoxic tumor regions.

Discussion

Since the discovery of HIF-1 and HREs as transcriptional controls in multiple genes [42], it has become evident that tumor hypoxia is associated with a more aggressive cancer phenotype [43]. In this study, we demonstrated for the first time that hypoxic regions in solid tumors

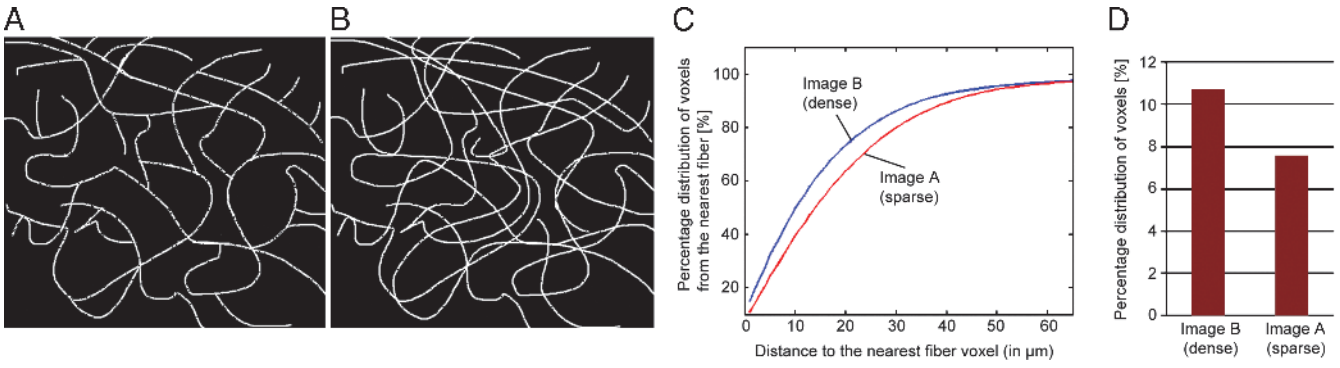

Figure 3. Performance of our software on a training data set of two artificial manually drawn fiber images of (A) sparser fibers and (B) denser fibers, in which just a few more lines representing fibers were added to image A. The software correctly detected (C) the shift toward a denser fiber distribution as well as (D) the increase in fiber volume in image B compared with that in image A.

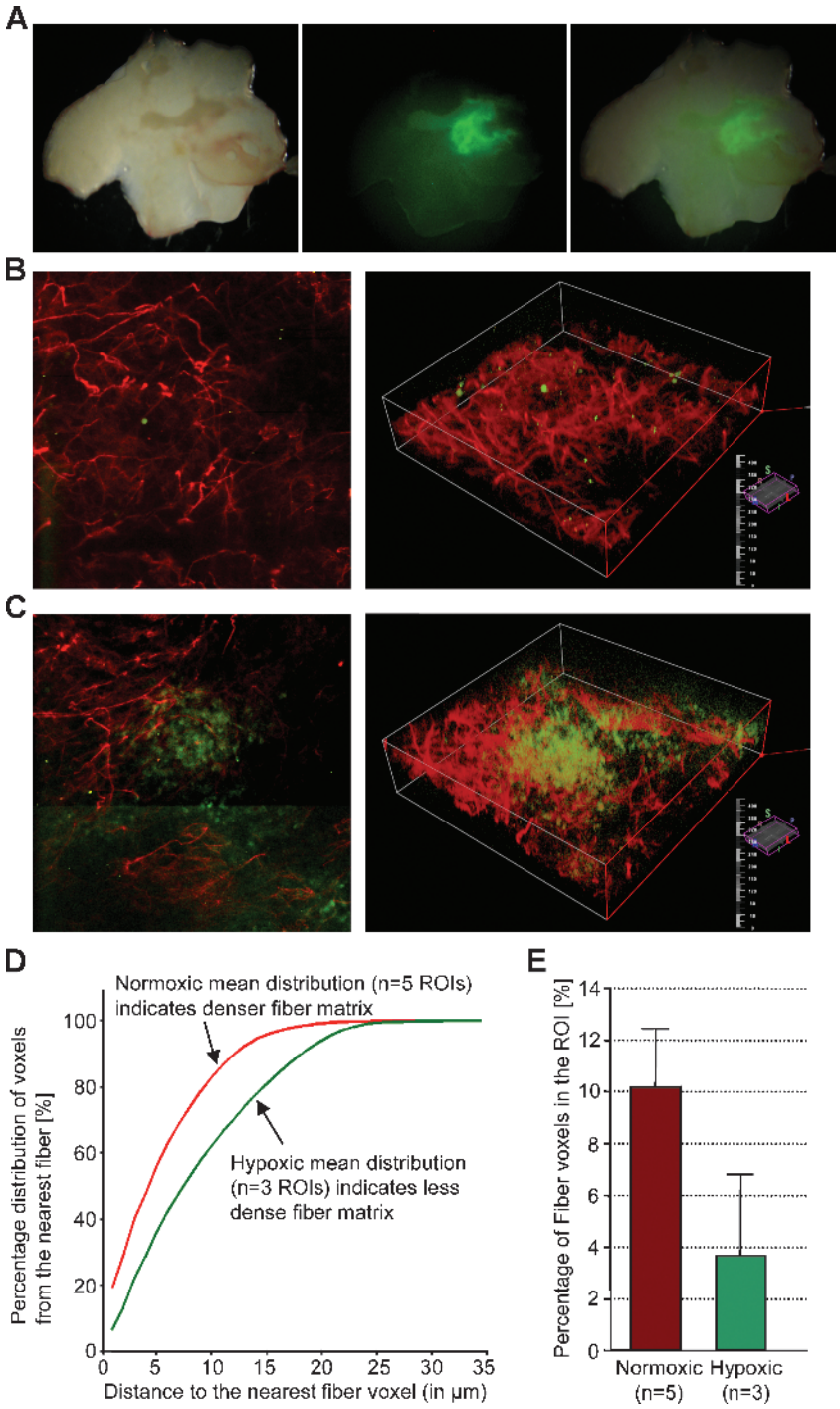

Figure 4. Hypoxic regions are heterogeneously distributed throughout MDA-MB-231 tumors as evident in a representative set of (A) bright-field, green fluorescence, and overlay microscopic images (left to right) of a fresh 2-mm-thick section from a solid MDA-MB-231–5HRE-EGFP breast tumor. Representative SHG Col1 fiber (red) and hypoxia (green) images are from (B) a normoxic and (C) a hypoxic FOV, displayed as *z*-projection (left) and as three-dimensionally reconstructed image (right). We computed (D) the mean distance distribution to the nearest fiber voxel as a measure of fiber density and (E) the percentage of fiber voxels within the ROI (mean ± SD). Data are from three tumors. Hypoxic regions had more than 80%, and normoxic regions had less than 1% of hypoxic EGFP-expressing cells in the ROI. Hypoxic tumor regions contained less dense and fewer Col1 fibers than normoxic regions in MDA-MB-231 breast tumor xenografts stably expressing HRE-EGFP.

contain significantly fewer and less dense Col1 fibers. We also developed a practical, intuitive, and robust image analysis approach to quantitatively characterize differences in Col1 fiber matrices and provide parameters that are visually evident, such as the Col1 fiber distance distribution and the Col1 fiber volume. Col1 fibers are the major structural ECM component in breast [4,10–12] and prostate tumors [8,13,14], and high Col1 fiber density and elevated Col1 synthesis have been associated with mammary tumor initiation, progression, and metastasis

[10,11] and prostate carcinogenesis [8]. Our data show that hypoxia significantly reduced the Col1 fiber matrix density in invasive, metastatic solid breast and prostate tumor models, whereas normoxic tumor regions contained a dense meshwork of Col1 fibers. Patient and animal model data associating increased fibrosis with elevated hypoxia do not contradict our current study because these studies did not compare hypoxic and normoxic regions within a given tumor but rather evaluated overall tumor hypoxia within a given tumor, based on staining

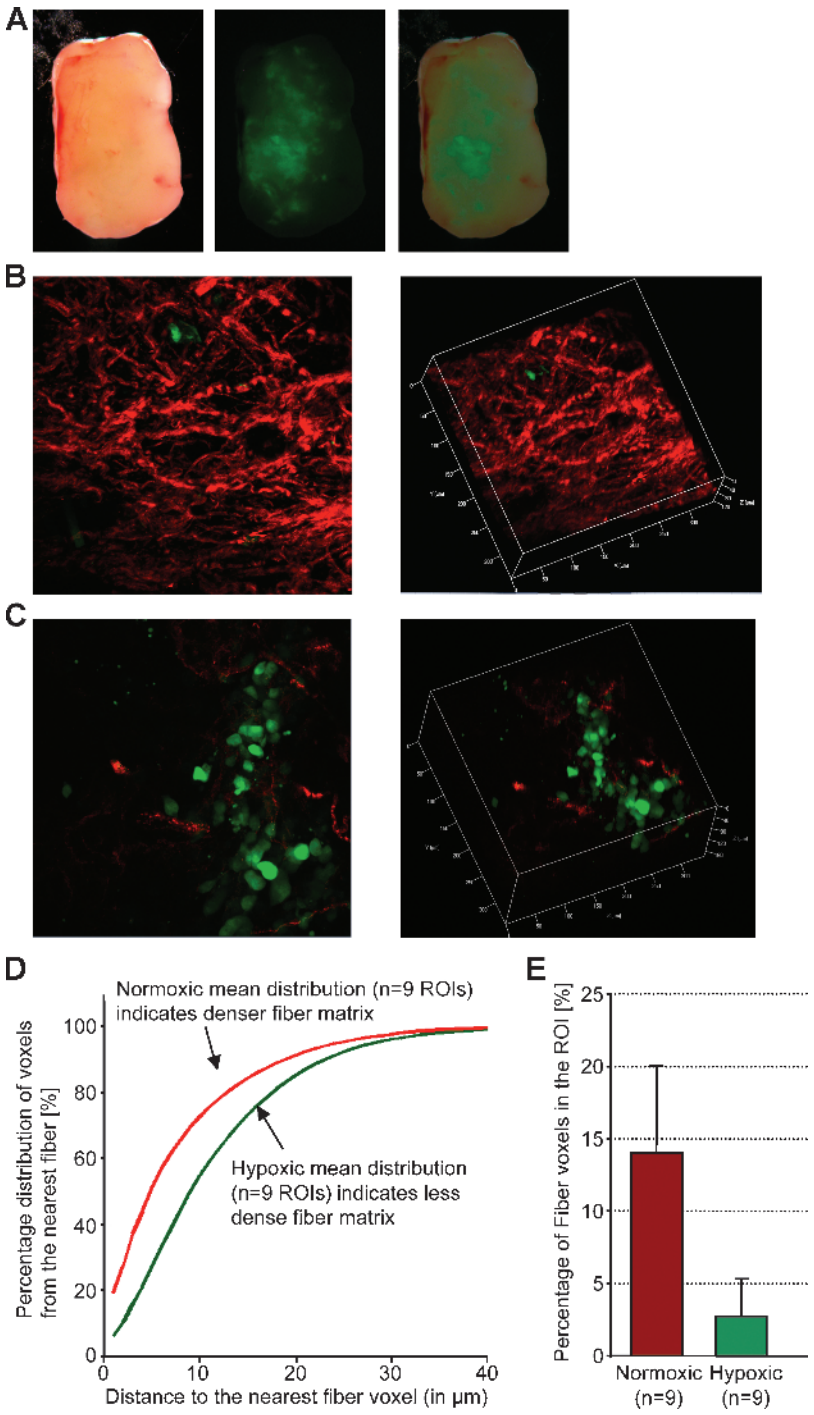

Figure 5. Consistent with Figure 2, hypoxic regions are heterogeneously distributed throughout solid PC-3 tumors as evident in a representative set of (A) bright-field, green fluorescence, and overlay microscopic images (left to right) of a fresh 2-mm-thick section from a solid PC-3–5HRE-EGFP prostate tumor. Representative SHG Col1 fiber (red) and hypoxia (green) images are from (B) a normoxic and (C) a hypoxic FOV, displayed as *z*-projection (left) and as three-dimensionally reconstructed image (right). We computed (D) the mean distance distribution to the nearest fiber voxel as a measure of fiber density and (E) the percentage of fiber voxels within the ROI (mean ± SD). Data are from three tumors. Hypoxic regions had more than 80%, and normoxic regions had less than 1% of hypoxic EGFP-expressing cells in the ROI. Hypoxic tumor regions contained less dense and fewer Col1 fibers than normoxic regions in PC-3 prostate tumor xenografts stably expressing HRE-EGFP.

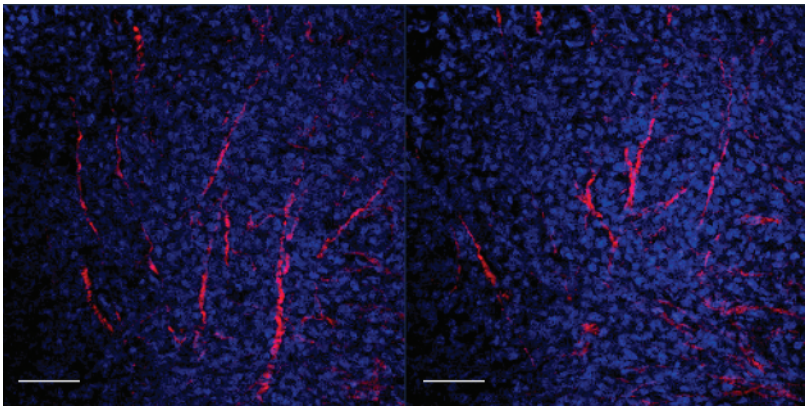

Figure 6. Representative *z*-sections of Hoechst 33342–stained whole-mount sections demonstrate that cells are evenly distributed throughout the tumors, independent of local fiber density. Col1 fibers are displayed in red, and nuclei are displayed in blue. Scale bars, 100 μm.

hypoxia markers, with respect to overall fibrosis staining in the same tumor [15–17]. Taken together, these findings indicate that although a dense Col1 matrix may be required for tumor initiation, its presence may not be necessary at later stages of tumor growth when hypoxia occurs. Our data suggest that once solid tumors are large enough for hypoxia to occur because of insufficient and chaotic vascularization, these hypoxic regions can acquire a loose and porous Col1 fiber matrix. Our previous validation of HRE-controlled expression of EGFP in cells in culture as well as in hypoxic tumor regions *in vivo* suggests that EGFP expression detected hypoxia of 1% or less that had existed for at least 6 hours and was within an oxygen tension of Po_2 less than 0.6 mm Hg [33]. Changes in the Col1 fiber matrix were therefore characterized in these chronically hypoxic regions. Future studies of the effects of acute hypoxia, reoxygenation, and transient hypoxia on the Col1 fiber matrix as well as the causative changes in gene expression will provide further insight into the regulation of Col1 fibers in tumors.

Col1 fiber degradation through proteolytic enzymes and reduced Col1 fiber synthesis are possible explanations for the less dense Col1 fiber matrix in hypoxic tumor regions. In terms of degradative processes, hypoxic conditions can increase the expression and activity of MMP-1 [44–46] and MMP-14 [47,48], especially in cancer cells. However, our microarray-based gene expression analysis in cell cultures revealed a reduction in MMP-3 or MMP-1 and MMP-16 expression on exposure to hypoxia in MDA-MB-231 breast or PC-3 prostate cancer cells, respectively. These cancer cell lines may behave differently under cell culture conditions compared with the *in vivo* situation in solid tumors. Further studies are necessary to compare the expression and activity levels of MMPs from cells within the tumor microenvironment, such as stromal fibroblasts, endothelial cells, and macrophages, among others. Other degradative pathways, such as the uPA-initiated cascade, may be involved in degrading Col1 fibers in hypoxic tumor regions. In this cascade, secreted uPA binds to cellular uPARs to catalyze the conversion of plasminogen to plasmin, which is a broad-spectrum enzyme that results in immediate ECM degradation or activation of multiple MMPs [28]. Hypoxic PC-3 cells in tissue culture showed higher uPA activity levels than oxygenated PC-3 cells [38]. Exposure of MDA-MB-231 cells to hypoxia was shown to increase uPAR expression along with increasing the invasiveness of these cells [49,50], which would support the possibility of uPAR-mediated Col1 degradation in hypoxic tumor regions.

In terms of Col1 synthesis, hypoxia has been found to stimulate Col1 fiber synthesis and cross-linking as outlined here. Hypoxia has been observed to activate the Col1A1 promoter through transforming growth factor β that is activated by HIF-1 [21,22] or by posttranscriptional processes [30]. Hypoxia was also shown to stimulate the expression of a cluster of hydroxylases required in the posttranslational processing of Col1 fibers [18]. Expression of these hydroxylases, such as prolyl-4-hydroxylases and procollagen lysyl-hydroxylase, may be coordinated by HIF-1 [18]. LOX, which cross-links Col1 microfibrils, has recently been implicated in hypoxia-induced metastasis [51,52]. LOX is regulated by HIF-1, and secreted LOX is responsible for the invasive/metastatic properties of hypoxic human cancer cells through focal adhesion kinase activity and cell-matrix adhesion [51,52]. The gene expression analysis in our study revealed a significant increase in LOX expression under hypoxia in invasive/metastatic breast and prostate cancer cells alike, which is in good agreement with these studies [51,52]. Co11 fiber density and volume will ultimately depend on the net balance between synthesis and degradation. The less dense, porous Col1 fiber matrix observed in hypoxic tumor regions suggests that degradation may have dominated over synthesis in chronically hypoxic tumor regions.

In summary, using combined SHG and fluorescence microscopy and a newly developed image analysis approach to quantify fiber structures,

Table 1. Genes of Secreted Factors That Are Involved in Col1 Synthesis and Breakdown and Contained on the Affymetrix Human Genome U133 Plus 2.0 Array, Which Are Differentially Expressed in Hypoxic *versus* Normoxic Human MDA-MB-231 Breast Cancer Cells.

Gene Group	Gene Title	Gene Symbol	Representative Public ID	Fold Change	*P*
Col1 synthesis/ cross-linking	Lysyl oxidase	*LOX*	NM_002317	5.2446	.9435
Matrix metalloproteases	Matrix metallopeptidase 3 (stromelysin 1, progelatinase)	*MMP3*	NM_002422	–3.9105	.7526

Table 2. Genes of Secreted Factors That Are Involved in Col1 Synthesis and Breakdown and Contained on the Affymetrix Human Genome U133 Plus 2.0 Array, Which Are Differentially Expressed in Hypoxic *versus* Normoxic Human PC-3 Prostate Cancer Cells.

Gene Group	Gene Title	Gene Symbol	Representative Public ID	Fold Change	*P*
Col1 synthesis/crosslinking	Lysyl oxidase	*LOX*	NM_002317	3.2023	1.000
Matrix metalloproteases	Matrix metalloproteinase 1 (interstitial collagenase)	*MMP1*	NM_002421	−1.9742	.9966
	Matrix metalloproteinase 16 (membrane-inserted)	*MMP16*	U79292	−2.1110	.9995
uPA system proteases	Plasminogen activator, urokinase receptor	*PLAUR*	U08839	2.1025	.9974

we have demonstrated that hypoxia resulted in a more porous and reduced Col1 fiber matrix in hypoxic regions of solid tumors *in vivo*. The use of SHG microscopic detection of Col1 fibers to assess ECM integrity, which is an intrinsic contrast mechanism, may prove clinically useful in the future in minimally invasive procedures, such as biopsies or ablations, in which a fiber-optic microendoscope can be implemented as part of the biopsy or ablation needle. In normal tissue, Col1 fibers and the ECM, in general, are structured to guide interstitial fluid to the lymphatics [53]. Whereas hypoxia undoubtedly alters Col1 fibers in these human tumor xenograft models, the role of this Col1 restructuring in macromolecular transport and mediating cancer cell dissemination requires further investigation.

Acknowledgments

The authors thank Scot Kuo for expert technical support with the microscopy studies on the Zeiss 710 NLO Meta confocal microscope equipped for multiphoton microscopy, Gary Cromwell for laboratory support, and David Bonekamp for his help in developing the Col1 fiber analysis software.

References

[1] Jain RK (1988). Determinants of tumor blood flow: a review. *Cancer Res* **48**, 2641–2658.

[2] Tatum JL, Kelloff GJ, Gillies RJ, Arbeit JM, Brown JM, Chao KS, Chapman JD, Eckelman WC, Fyles AW, Giaccia AJ, et al. (2006). Hypoxia: importance in tumor biology, noninvasive measurement by imaging, and value of its measurement in the management of cancer therapy. *Int J Radiat Biol* **82**, 699–757.

[3] Hockel M and Vaupel P (2001). Tumor hypoxia: definitions and current clinical, biologic, and molecular aspects. *J Natl Cancer Inst* **93**, 266–276.

[4] Lochter A and Bissell MJ (1995). Involvement of extracellular matrix constituents in breast cancer. *Semin Cancer Biol* **6**, 165–173.

[5] Chung LW, Baseman A, Assikis V, and Zhau HE (2005). Molecular insights into prostate cancer progression: the missing link of tumor microenvironment. *J Urol* **173**, 10–20.

[6] Pathak AP, Artemov D, Neeman M, and Bhujwalla ZM (2006). Lymph node metastasis in breast cancer xenografts is associated with increased regions of extravascular drain, lymphatic vessel area, and invasive phenotype. *Cancer Res* **66**, 5151–5158.

[7] Alexandrakis G, Brown EB, Tong RT, McKee TD, Campbell RB, Boucher Y, and Jain RK (2004). Two-photon fluorescence correlation microscopy reveals the two-phase nature of transport in tumors. *Nat Med* **10**, 203–207.

[8] Tuxhorn JA, Ayala GE, Smith MJ, Smith VC, Dang TD, and Rowley DR (2002). Reactive stroma in human prostate cancer: induction of myofibroblast phenotype and extracellular matrix remodeling. *Clin Cancer Res* **8**, 2912–2923.

[9] Cooper CR, Chay CH, Gendernalik JD, Lee HL, Bhatia J, Taichman RS, McCauley LK, Keller ET, and Pienta KJ (2003). Stromal factors involved in prostate carcinoma metastasis to bone. *Cancer* **97**, 739–747.

[10] Provenzano PP, Eliceiri KW, Campbell JM, Inman DR, White JG, and Keely PJ (2006). Collagen reorganization at the tumor-stromal interface facilitates local invasion. *BMC Med* **4**, 38.

[11] Provenzano PP, Inman DR, Eliceiri KW, Knittel JG, Yan L, Rueden CT, White JG, and Keely PJ (2008). Collagen density promotes mammary tumor initiation and progression. *BMC Med* **6**, 11.

[12] Li T, Sun L, Miller N, Nicklee T, Woo J, Hulse-Smith L, Tsao MS, Khokha R, Martin L, and Boyd N (2005). The association of measured breast tissue characteristics with mammographic density and other risk factors for breast cancer. *Cancer Epidemiol Biomarkers Prev* **14**, 343–349.

[13] Taboga SR and Vidal Bde C (2003). Collagen fibers in human prostatic lesions: histochemistry and anisotropies. *J Submicrosc Cytol Pathol* **35**, 11–16.

[14] Zhang Y, Nojima S, Nakayama H, Jin Y, and Enza H (2003). Characteristics of normal stromal components and their correlation with cancer occurrence in human prostate. *Oncol Rep* **10**, 207–211.

[15] Colpaert CG, Vermeulen PB, Fox SB, Harris AL, Dirix LY, and Van Marck EA (2003). The presence of a fibrotic focus in invasive breast carcinoma correlates with the expression of carbonic anhydrase IX and is a marker of hypoxia and poor prognosis. *Breast Cancer Res Treat* **81**, 137–147.

[16] Van den Eynden GG, Colpaert CG, Couvelard A, Pezzella F, Dirix LY, Vermeulen PB, Van Marck EA, and Hasebe T (2007). A fibrotic focus is a prognostic factor and a surrogate marker for hypoxia and (lymph)angiogenesis in breast cancer: review of the literature and proposal on the criteria of evaluation. *Histopathology* **51**, 440–451.

[17] McPhail LD and Robinson SP (2010). Intrinsic susceptibility MR imaging of chemically induced rat mammary tumors: relationship to histologic assessment of hypoxia and fibrosis. *Radiology* **254**, 110–118.

[18] Hofbauer KH, Gess B, Lohaus C, Meyer HE, Katschinski D, and Kurtz A (2003). Oxygen tension regulates the expression of a group of procollagen hydroxylases. *Eur J Biochem* **270**, 4515–4522.

[19] Shoulders MD and Raines RT (2009). Collagen structure and stability. *Annu Rev Biochem* **78**, 929–958.

[20] Corpechot C, Barbu V, Wendum D, Kinnman N, Rey C, Poupon R, Housset C, and Rosmorduc O (2002). Hypoxia-induced VEGF and collagen I expressions are associated with angiogenesis and fibrogenesis in experimental cirrhosis. *Hepatology* **35**, 1010–1021.

[21] Rossert J, Terraz C, and Dupont S (2000). Regulation of type I collagen genes expression. *Nephrol Dial Transplant* **15**(suppl 6), 66–68.

[22] Gong LM, Du JB, Shi L, Shi Y, and Tang CS (2004). Effects of endogenous carbon monoxide on collagen synthesis in pulmonary artery in rats under hypoxia. *Life Sci* **74**, 1225–1241.

[23] Kauppila S, Stenback F, Risteli J, Jukkola A, and Risteli L (1998). Aberrant type I and type III collagen gene expression in human breast cancer *in vivo*. *J Pathol* **186**, 262–268.

[24] Kao RT, Hall J, and Stern R (1986). Collagen and elastin synthesis in human stroma and breast carcinoma cell lines: modulation by the extracellular matrix. *Connect Tissue Res* **14**, 245–255.

[25] Sabeh F, Ota I, Holmbeck K, Birkedal-Hansen H, Soloway P, Balbin M, Lopez-Otin C, Shapiro S, Inada M, Krane S, et al. (2004). Tumor cell traffic through the extracellular matrix is controlled by the membrane-anchored collagenase MT1-MMP. *J Cell Biol* **167**, 769–781.

[26] Coussens LM, Fingleton B, and Matrisian LM (2002). Matrix metalloproteinase inhibitors and cancer: trials and tribulations. *Science* **295**, 2387–2392.

[27] Egeblad M and Werb Z (2002). New functions for the matrix metalloproteinases in cancer progression. *Nat Rev Cancer* **2**, 161–174.

[28] Andreasen PA, Kjoller L, Christensen L, and Duffy MJ (1997). The urokinase-type plasminogen activator system in cancer metastasis: a review. *Int J Cancer* **72**, 1–22.

[29] Falanga V, Zhou L, and Yufit T (2002). Low oxygen tension stimulates collagen synthesis and COL1A1 transcription through the action of TGF-beta1. *J Cell Physiol* **191**, 42–50.

[30] Horino Y, Takahashi S, Miura T, and Takahashi Y (2002). Prolonged hypoxia accelerates the posttranscriptional process of collagen synthesis in cultured fibroblasts. *Life Sci* **71**, 3031–3045.

[31] Brown E, McKee T, diTomaso E, Pluen A, Seed B, Boucher Y, and Jain RK (2003). Dynamic imaging of collagen and its modulation in tumors *in vivo* using second-harmonic generation. *Nat Med* **9**, 796–800.

[32] Falzon G, Pearson S, and Murison R (2008). Analysis of collagen fibre shape changes in breast cancer. *Phys Med Biol* **53**, 6641–6652.

[33] Raman V, Artemov D, Pathak AP, Winnard PT Jr, McNutt S, Yudina A, Bogdanov A Jr, and Bhujwalla ZM (2006). Characterizing vascular parameters in hypoxic regions: a combined magnetic resonance and optical imaging study of a human prostate cancer model. *Cancer Res* **66**, 9929–9936.

[34] Glunde K, Shah T, Winnard PT Jr, Raman V, Takagi T, Vesuna F, Artemov D, and Bhujwalla ZM (2008). Hypoxia regulates choline kinase expression through hypoxia-inducible factor-1 alpha signaling in a human prostate cancer model. *Cancer Res* **68**, 172–180.

[35] Cailleau R, Young R, Olive M, and Reeves WJ Jr (1974). Breast tumor cell lines from pleural effusions. *J Natl Cancer Inst* **53**, 661–674.

[36] Kaighn ME, Narayan KS, Ohnuki Y, Lechner JF, and Jones LW (1979). Establishment and characterization of a human prostatic carcinoma cell line (PC-3). *Invest Urol* **17**, 16–23.

[37] Glunde K, Jie C, and Bhujwalla ZM (2004). Molecular causes of the aberrant choline phospholipid metabolism in breast cancer. *Cancer Res* **64**, 4270–4276.

[38] Ackerstaff E, Artemov D, Gillies RJ, and Bhujwalla ZM (2007). Hypoxia and the presence of human vascular endothelial cells affect prostate cancer cell invasion and metabolism. *Neoplasia* **9**, 1138–1151.

[39] Glunde K, Foss CA, Takagi T, Wildes F, and Bhujwalla ZM (2005). Synthesis of 6′-*O*-lissamine-rhodamine B-glucosamine as a novel probe for fluorescence imaging of lysosomes in breast tumors. *Bioconjug Chem* **16**, 843–851.

[40] Irizarry RA, Hobbs B, Collin F, Beazer-Barclay YD, Antonellis KJ, Scherf U, and Speed TP (2003). Exploration, normalization, and summaries of high density oligonucleotide array probe level data. *Biostatistics* **4**, 249–264.

[41] Bolstad BM, Irizarry RA, Astrand M, and Speed TP (2003). A comparison of normalization methods for high density oligonucleotide array data based on variance and bias. *Bioinformatics* **19**, 185–193.

[42] Semenza GL (2000). Expression of hypoxia-inducible factor 1: mechanisms and consequences. *Biochem Pharmacol* **59**, 47–53.

[43] Semenza GL (2002). HIF-1 and tumor progression: pathophysiology and therapeutics. *Trends Mol Med* **8**, S62–S67.

[44] Cha HS, Ahn KS, Jeon CH, Kim J, Song YW, and Koh EM (2003). Influence of hypoxia on the expression of matrix metalloproteinase-1, -3 and tissue inhibitor of metalloproteinase-1 in rheumatoid synovial fibroblasts. *Clin Exp Rheumatol* **21**, 593–598.

[45] Guo WJ, Li J, Chen Z, Zhuang JY, Gu WH, Zhang L, Pang J, Lu CH, Zhang WZ, and Cheng YF (2004). Transient increased expression of VEGF and MMP-1 in a rat liver tumor model after hepatic arterial occlusion. *Hepatogastroenterology* **51**, 381–386.

[46] Kan C, Abe M, Yamanaka M, and Ishikawa O (2003). Hypoxia-induced increase of matrix metalloproteinase-1 synthesis is not restored by reoxygenation in a three-dimensional culture of human dermal fibroblasts. *J Dermatol Sci* **32**, 75–82.

[47] Kondo S, Kubota S, Shimo T, Nishida T, Yosimichi G, Eguchi T, Sugahara T, and Takigawa M (2002). Connective tissue growth factor increased by hypoxia may initiate angiogenesis in collaboration with matrix metalloproteinases. *Carcinogenesis* **23**, 769–776.

[48] Ottino P, Finley J, Rojo E, Ottlecz A, Lambrou GN, Bazan HE, and Bazan NG (2004). Hypoxia activates matrix metalloproteinase expression and the VEGF system in monkey choroid-retinal endothelial cells: involvement of cytosolic phospholipase A2 activity. *Mol Vis* **10**, 341–350.

[49] Graham CH, Forsdike J, Fitzgerald CJ, and Macdonald-Goodfellow S (1999). Hypoxia-mediated stimulation of carcinoma cell invasiveness via upregulation of urokinase receptor expression. *Int J Cancer* **80**, 617–623.

[50] Lash GE, Fitzpatrick TE, and Graham CH (2001). Effect of hypoxia on cellular adhesion to vitronectin and fibronectin. *Biochem Biophys Res Commun* **287**, 622–629.

[51] Erler JT, Bennewith KL, Nicolau M, Dornhofer N, Kong C, Le QT, Chi JT, Jeffrey SS, and Giaccia AJ (2006). Lysyl oxidase is essential for hypoxia-induced metastasis. *Nature* **440**, 1222–1226.

[52] Erler JT and Giaccia AJ (2006). Lysyl oxidase mediates hypoxic control of metastasis. *Cancer Res* **66**, 10238–10241.

[53] Pepper MS, Tille JC, Nisato R, and Skobe M (2003). Lymphangiogenesis and tumor metastasis. *Cell Tissue Res* **314**, 167–177.